Available online at www.sciencedirect.com
ScienceDirect
Aerosol Science 39 (2008) 888–896
Journal of Aerosol Science
www.elsevier.com/locate/jaerosci

Technical note

Spark generation of monometallic and bimetallic aerosol nanoparticles

Jeong Hoon Byeon, Jae Hong Park, Jungho Hwang*

Department of Mechanical Engineering, Yonsei University, Seoul 120-749, Republic of Korea

Received 18 January 2008; received in revised form 30 April 2008; accepted 19 May 2008

Abstract

This paper reports the generation and characterization of monometallic (palladium (Pd), platinum (Pt), gold (Au), and silver (Ag) from electrodes of the same material) and bimetallic (Pd–Pt, Pd–Au, and Pd–Ag from electrodes of different materials) aerosol particles produced using a spark discharge. The Ag, Pd, Pt, and Au monometallic particles were agglomerates with a mean diameter of 14.9, 26.7, 37.7, and 48.8 nm, respectively. The agglomerates consisted of primary particles ranging in size from 2 to 4 nm (Ag < Pd < Pt < Au). The corresponding rates of particle generation were 0.12, 1.68, 16.00, and 40.30 μg/min. A hypothesis was suggested that there is a correlation between the generation rate and the ionization potential of a metal (Ag < Pd < Pt < Au). The bimetallic particles were found to be binary mixtures (not alloys) of two individual monometallic particles. The compositions of the bimetallic particles were measured at different combinations of materials and polarity of the spark electrode. When the ionization potential of an anode material was higher than that of a cathode material, the hypothesis that there is a correlation between the ionization potential and the generation rate was valid. Even if the ionization potential of the anode material was lower than that of the cathode material, the generation rate of the anode metal particles was higher than that of the cathode metal particles. This might be caused by higher temperature channel formed near the anode and thus higher evaporation and subsequent nucleation/condensation near the anode.
© 2008 Elsevier Ltd. All rights reserved.

Keywords: Spark generation; Monometallic particles; Bimetallic particles; Particle generation rate; Spark electrode polarity

1. Introduction

The generation of metallic nanoparticles has mainly been carried out in liquid solutions containing metal ions, reductants, and some polymers (protecting agents) (Devarajan, Bera, & Sampath, 2005). Recently, considerable attention has been focused on the characteristics of "naked" metal nanoparticles (Harada, Toshima, Yoshida, & Isoda, 2005), which are believed to be appropriate for examining the effect of surface structure and geometry. However, the addition of both reducing and protecting agents highlights the complexity of their generation (Yang, Wan, & Wang, 2004). Other methods for generating naked metallic nanoparticles include pyrolysis, chemical vapor deposition, and sputtering. However, these processes demand either high temperatures or a high vacuum environment, which are expensive to operate (Lu & Lin, 2000).

Spark generation has been used to generate monometallic particles of a wide range of conducting materials with particles sizes ranging from several nanometers up to ~ 100 m in an aerosol state because spark generation is simple,

* Corresponding author. Fax: +82 2 312 2821.
E-mail address: hwangjh@yonsei.ac.kr (J. Hwang).

0021-8502/$ - see front matter © 2008 Elsevier Ltd. All rights reserved.
doi:10.1016/j.jaerosci.2008.05.006

easily deliverable, and environmental friendly (Borra, 2006; Evans, Harrison, & Ayres, 2003; Horvath & Gangl, 2003; Kim & Chang, 2005; Schwyn, Garwin, & Schmidt-Ott, 1988; Simonin, Lafont, Tabrizi, Schmidt-Ott, & Kelder, 2007; Watters, Jr., DeVoe, Shen, Small, & Marinenko, 1989). While most of these studies introduced specific metal particles by spark generation for particular applications, few studies have discussed the aerosol behavior of these particles with the exception of Evans et al. (2003), Horvath and Gangl (2003), Kim and Chang (2005), and Schwyn et al. (1988), who measured the particle size distribution using a scanning mobility particle sizer (SMPS). However, the mechanisms of particle synthesis are not completely understood.

This paper reports the production of monometallic (palladium (Pd), platinum (Pt), gold (Au), and silver (Ag)) and bimetallic (Pd–Pt, Pd–Au, and Pd–Ag) aerosol particles using homogeneous and heterogeneous spark generation, respectively. The size distribution, rate of generation, morphology, and structure of the particles were characterized by SMPS, scanning electron microscopy (SEM)—energy dispersive X-ray spectroscopy (EDX), transmission electron microscopy (TEM)—selected area electron diffraction (SAED), inductively coupled plasma atomic emission spectroscopy (ICPAES), and X-ray diffraction (XRD) methods. The synthesis mechanisms of the monometallic and bimetallic particles are also discussed.

2. Experimental

Fig. 1 shows a schematic of the spark generation process. A spark was generated between two either identical (homogeneous spark) or different (heterogeneous spark) metal rods (diameter: 3 mm, length: 100 mm, Nilaco, Japan) inside a reactor (volume: 42.8 cm^3) under a pure nitrogen environment (less than 10^{-4} impurities) at STP (Byeon et al., 2006). The flow rate of nitrogen gas, which was controlled using a mass flow controller (MKS, USA), was set to 3 L/min. The electrical circuit specifications are as follows: a resistance of 0.5 MΩ, a capacitance of 10 nF, a loading current of 2 mA, an applied voltage of 3.0 kV, and a frequency of 667 Hz. The gas temperature inside the spark channel was increased beyond a critical value (Berkowitz & Walter, 1987; Borra, 2006), which was sufficient to sublimate parts of the electrodes. The duration of each spark was very short (∼1.5 ms) and the vapors cooled rapidly downstream of the spark. This formed a supersaturation resulting particle formation through nucleation/condensation. The generated particles were carried using a flow of nitrogen gas and then sampled on a carbon-coated copper grid (for use in TEM–SAED and SEM–EDX analyses), a glass fiber (for use in XRD analyses), or a polytetrafluoroethylene (PTFE) membrane filter (for use in ICPAES analyses) at 20 cm downstream of the spark generator. The spark generator was cleaned periodically with compressed dry particle-free air to eliminate the residual particles. The effluents from the sampler were passed through a high efficiency particulate air (HEPA) filter to remove the non-sampled particles before releasing them into the laboratory hood through an exhaust system.

The size distribution of the spark generated particles was measured using a SMPS system consisting of an electrostatic classifier (3085, TSI, USA), condensation particle counter (CPC, 3025, TSI, USA), and aerosol charge neutralizer

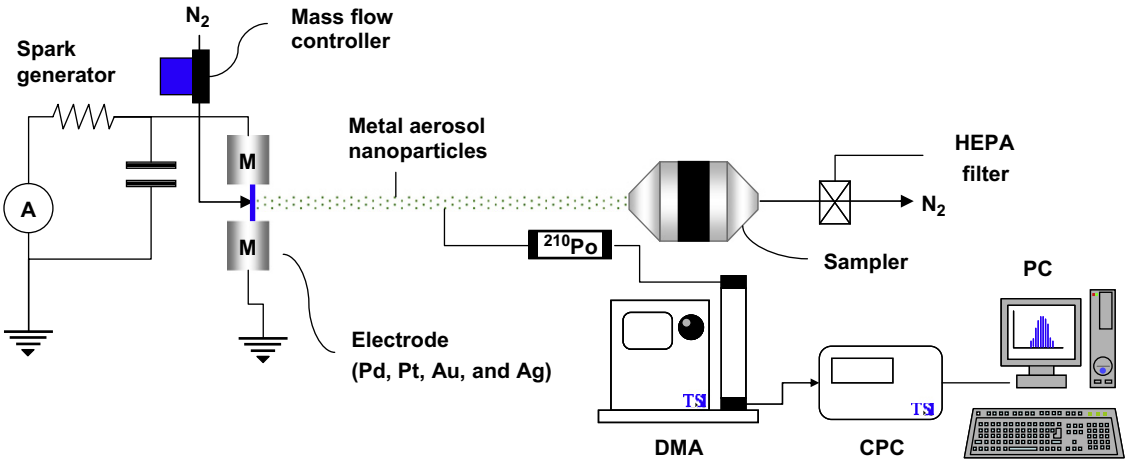

Fig. 1. Schematic of experimental setup.

(Po-210, NRD, USA). The SMPS system was operated with a sample flow of 0.3 L/min, a sheath flow of 3 L/min, and a scan time of 180 s (measurement range: 4.61–157 nm). The morphology and corresponding SAED patterns of the particles were analyzed by high-resolution TEM (HRTEM, JEM-3010, JEOL, Japan) operated at 300 kV. The field-emission SEM (FESEM, JSM-6500F, JEOL, Japan) images and EDX (JED-2300, JEOL, Japan) profiles were obtained at an accelerating voltage of 15 kV. The rate of generation and metal content of the particles were determined by ICPAES (Elan 6000, Perkin-Elmer, USA). A particle-sampled PTFE membrane filter was dipped in a concentrated acid medium (18 M H_2SO_4, 22 M HF, 16 M HNO_3). The metal content was obtained by a comparison with standard solutions in the same medium. XRD of the particles were carried out on a Rigaku RINT-2100 diffractometer equipped with a thin-film attachment using Cu-Kα radiation (40 kV, 40 mA). The 2θangles ranged from 10° to 100° with a scan rate of 4°/min by step scanning at an interval of 0.08°. The particle size of the metal was calculated from the XRD spectra in accordance with Scherrer's formula ($t = 0.9\lambda/(B\cos\theta)$).

3. Results and discussion

Fig. 2 shows the size distribution of the spark generated monometallic (Pd, Pt, Au, and Ag) aerosol particles. The particle concentrations were different(Au > Pt > Pd > Ag), even though the electric power was constant as 6 wt for spark at 667 Hz. Detail parameters of the size distributions are summarized in Table 1. The generation rates of Ag, Pd, Pt, and Au particles were 0.12, 1.68, 16.00, and 40.30 μg/min, respectively.

Fig. 3 shows the morphology, composition, and structure of the Pd and Au monometallic particles. Both SEM micrographs (Fig. 3a) show the mean sizes of the Pd and Au particles to be ∼25 and ∼45 nm, respectively, which agrees well with the SMPS data shown in Fig. 2. Fig. 3a also shows the EDX profiles of the particles, which contained peaks for Pd and Au, respectively. Fig. 3b shows TEM micrographs, from which the white spots in the SEM micrographs

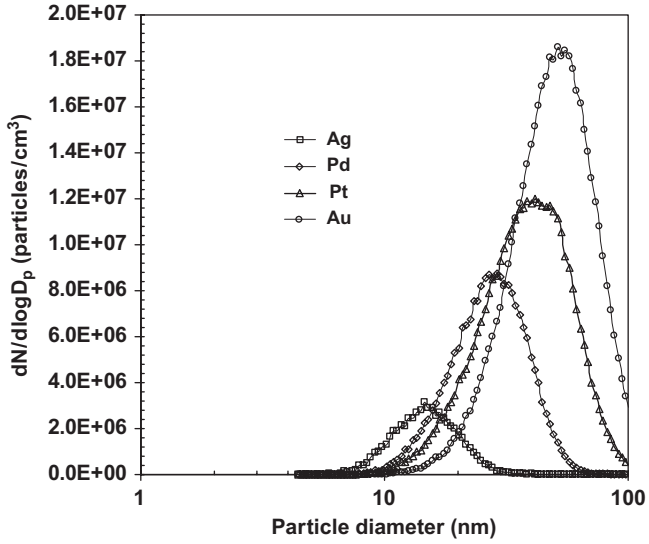

Fig. 2. Particle size distribution of monometallic particles.

Table 1
Size distribution of monometallic particles

	Ag	Pd	Pt	Au
Geometric mean diameter (nm)	14.91	26.66	37.68	48.79
Geometric standard deviation	1.38	1.43	1.53	1.48
Total concentration (cm^{-3})	9.45E + 05	3.36E + 06	5.60E + 06	7.75E + 06
Total surface particle area (nm^2/cm^3)	1.80E + 08	1.92E + 09	6.91E + 09	1.54E + 10

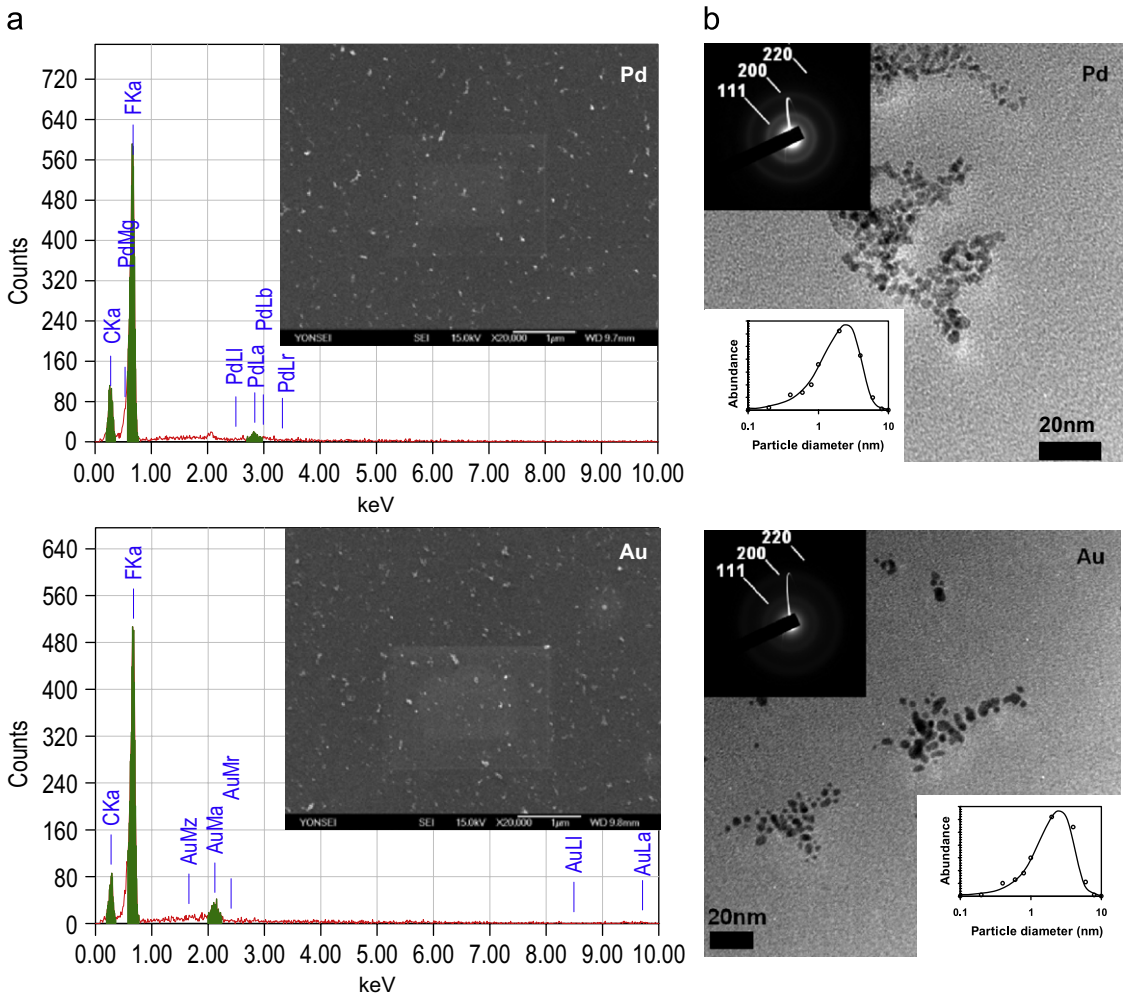

Fig. 3. Morphology, composition, and structure of Pd and Au monometallic particles. (a) SEM micrographs and EDX profiles. (b) TEM micrographs and SAED patterns.

were agglomerates consisting of primary Pd and Au particles. Fig. 3b also shows the size distribution of the primary particles. The mean diameter of the Pd and Au primary particles were 2.6 and 3.5 nm, respectively. The SAED patterns (also shown in Fig. 3b) of Pd and Au particles showed clear diffraction Debye–Scherrer rings of the [1 1 1] and [2 0 0] reflections and a weak diffraction ring of the [2 2 0] reflection. Fig. 4 shows the X-ray diffractions of Pd, Pt, Au, and Ag particles. Four characteristic peaks for Pd ($2\theta = 40.1$, 46.7, 68.1, and 82.1°), Pt ($2\theta = 39.8$, 46.2, 67.4, and 81.3°), Au ($2\theta = 38.2$, 44.4, 64.6, and 77.5°), and Ag ($2\theta = 38.1$, 44.3, 64.4, and 77.5°) were observed and marked by the [1 1 1], [2 0 0], [2 2 0], and [3 1 1] planes. The SAED patterns and XRD data indicate that the spark generated Pd and Au particles were face-centered cubic (fcc) crystallites. The peak intensity was the highest for Au on account of its largest amount and size (refer to Fig. 2). The average particle sizes estimated from XRD line broadening of the [1 1 1] peak, according to Scherrer's formula, were 1.6, 2.1, 2.4, and 3.4 nm for Ag, Pd, Pt, and Au, respectively. The average sizes were slightly smaller than those obtained by TEM, due to interference of the glass fiber containing SiO_2 and impurities during the XRD measurement.

Obtaining these primary metal particles by spark generation requires the growth of clusters with a magic number (Oleshko, 2006), $N = 1/3(10m^3 + 15m^2 + 11m + 3)$, of metal atoms filling a layer around the central atom, where m is the number of metal layers. A spark channel is formed when the applied voltage is beyond a critical value. This results in the generation of energetic electrons and ions (Artamonov, Krasov, & Paperny, 2001; Holland, 1956; Krasik et al., 2006;

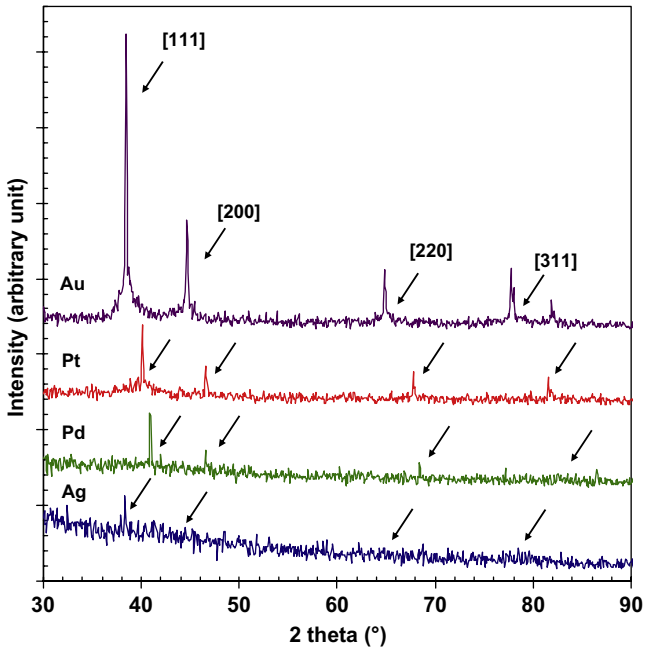

Fig. 4. XRD pattern of monometallic particles.

Table 2
Parameter of monometallic particle generation

Element	Melting temperature (K)	Relative sputtering rate	Ionization potential (eV)
Ag	1234.9	1.20	7.58
Pd	1828.0	0.85	8.33
Pt	2041.4	0.60	9.00
Au	1337.3	1.00	9.22

Marusina & Filimonenko, 1984), which collide with the anode and cathode (Borra, Goldman, Goldman, & Boulaud, 1998), respectively. Metal atoms are detached from the electrodes by ion bombardment (sputtering). Some of the atoms can be ionized after being collided by energetic electrons. Consequently, the ionized metals with electrons and neutral metals can co-exist in direct spatial coincidence near the channel (Krasik et al., 2006). Since a high temperature spark channel is formed (Berkowitz & Walter, 1987; Borra, 2006), a part of the electrodes can evaporate. These gaseous metals are transported downstream of the spark channel by the nitrogen gas flow, where the primary particles are formed under the condition of high supersaturation and subsequent nucleation/condensation (Borra, 2006). Therefore, the plausible parameters for metal particle generation are the melting temperature, sputtering rate (Mizsei, Sipilä, & Lantto, 1998; Quorum Technologies, 2007), and ionization potential (Neogrády, Kellö, Urban, & Sadlej, 1997) of the metals. The ionization potential of an atom is the energy required to remove of electrons from isolated gaseous atoms, and a higher ionization potential of the material favors atom enrichment (Harada et al., 2005; Wang, Chung, & Perng, 2006) near the spark channel. Table 2 shows the parameters for Ag, Pd, Pt and Au. The highest ionization potential of Au atom (9.22 eV) suggests that Au tends to remain in the neutral state. Therefore, the largest amount of Au atoms can be formed before the formation of clusters and primary particles of Au. The results imply a hypothesis that there is a correlation between the ionization potential and the generation rate.

Fig. 5 shows the size distribution of spark generated bimetallic aerosol particles. Detail parameters of the size distributions are summarized in Table 3. The size distribution for any bimetal combination was between the size distributions of the two monometallic cases (see Fig. 2), which suggests the simple mixing of two individual spark

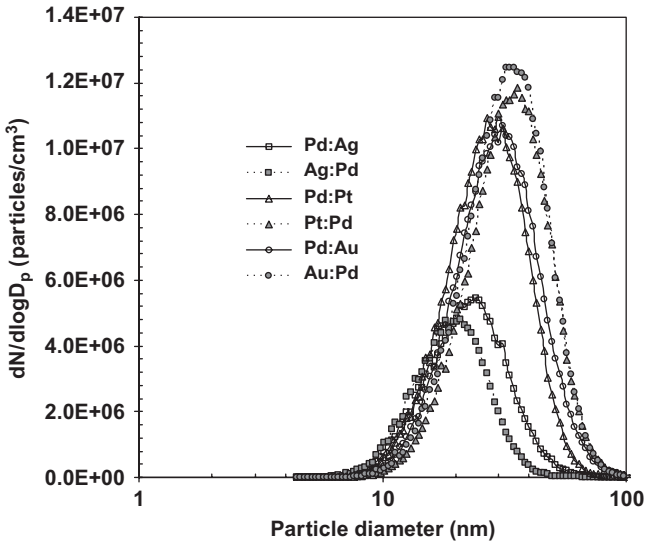

Fig. 5. Particle size distribution of bimetallic particles.

Table 3
Size distribution of bimetallic particles

Anode(+) : cathode(−)	Pd:Ag	Ag:Pd	Pd:Pt	Pt:Pd	Pd:Au	Au:Pd
Geometric mean diameter (nm)	22.07	19.01	28.42	32.32	29.15	31.65
Geometric standard deviation	1.46	1.41	1.45	1.46	1.48	1.47
Total concentration (cm^{-3})	2.20E + 06	1.78E + 06	4.41E + 06	4.76E + 06	4.45E + 06	5.20E + 06
Total surface particle area (nm^2/cm^3)	1.01E + 09	5.21E + 08	2.19E + 10	4.09E + 09	3.12E + 09	4.31E + 09

Table 4
Metal fraction and generation rate of bimetallic particles

Element (anode(+) : cathode(−))	Mass fraction	Particle generation rate (μg/ min)
Pd:Ag	0.85:0.15	0.66
Ag:Pd	0.25:0.75	0.28
Pd:Pt	0.52:0.47	2.64
Pt:Pd	0.68:0.32	6.28
Pd:Au	0.59:0.41	3.78
Au:Pd	0.70:0.30	6.88

generated materials. The polarity of the electrodes in each bimetal combination strongly affected the size distribution. Table 4 shows the corresponding mass fractions and generation rates. When the ionization potential of an anode material was higher than that of a cathode material, the hypothesis that there is a correlation between the ionization potential and the generation rate was valid. It is interesting that even if the ionization potential of the anode material was lower than that of the cathode material, the generation rate of the anode metal particles was higher than that of the cathode metal particles. This might be caused by higher temperature channel formed near the anode and thus higher evaporation and subsequent nucleation/condensation near the anode (Artamonov et al., 2001; Borra et al., 1998; Krasik et al., 2006). On the other hand, for the Pd–Ag sparks (Ag(+) : Pd(−) and Pd(+) : Ag(−)), Pd always had a higher fraction than Ag regardless of the electrode polarity. This might be due to the large difference in the concentrations of Ag and Pd, as shown in Table 1.

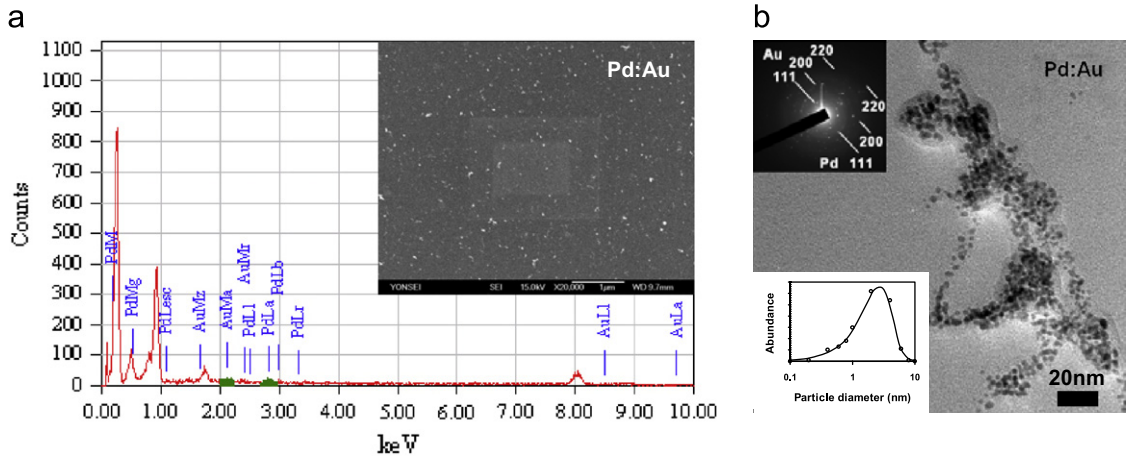

Fig. 6. Morphology, composition, and structure of Pd:Au bimetallic particles. (a) SEM micrograph and EDX profile. (b) TEM micrograph and SAED pattern.

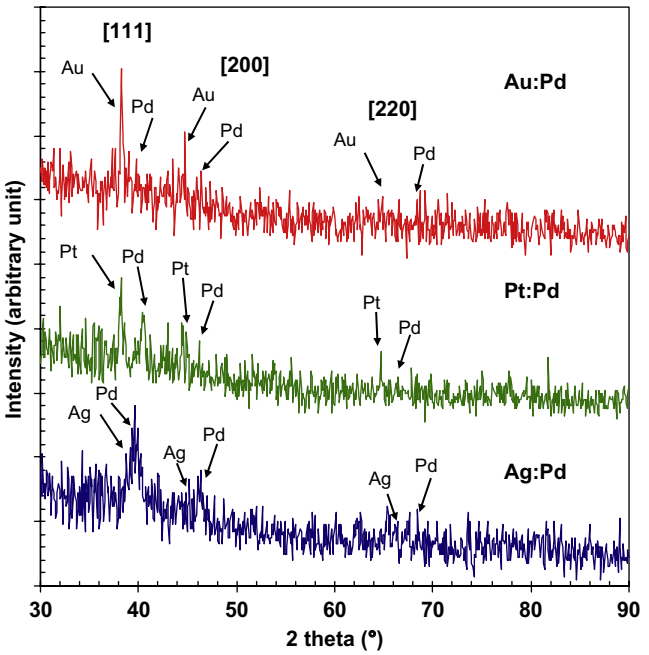

Fig. 7. XRD pattern of bimetallic particles.

Fig. 6 shows the morphology, composition, and structure of the bimetallic Pd(+) : Au(−) particles. SEM (Fig. 6a) shows that the mean size of the particles was approximately 34 nm, which corresponds to the results shown in Table 3 (29.15 nm). The corresponding EDX profile shows that both Pd and Au particles were contained in the agglomerated particles. TEM (Fig. 6b) showed that the bimetallic particles consisted of primary particles of almost uniform size (2–4 nm) but it could not be determined if the primary particles were a binary mixture or an alloy. Fig. 6b also shows the corresponding SAED pattern to the TEM micrograph. This pattern consists of overlapping rings of individual monometallic particles of Pd and Au, showing [1 1 1], [2 0 0], and [2 2 0] reflections of the fcc lattice of monometallic Pd and Au. This SAED pattern suggests that the Pd:Au particles obtained were not alloys but had a structure similar to the combined structure of monometallic Pd and Au particles.

In order to determine if the bimetallic particles were a binary mixture or an alloy, the XRD patterns (Fig. 7) of the Ag(+) : Pd(−), Pt(+) : Pd(−), and Au(+) : Pd(−) particles were obtained. The diffraction patterns of all bimetallic particles consisted of two consecutive peaks at [1 1 1], [2 0 0], and [2 2 0] planes for the two individual materials. The XRD patterns did not show any other additional peaks other than those for the two mono metals, indicating that a simple binary metal mixture had been formed instead of an alloy. Therefore, particles existed stably as a monometallic phase during heterogeneous spark generation even though they had agglomerated. Peak broadening analyses of the [1 1 1] peaks of all bimetallic particles indicated an average crystal size ranging from 1 to 3 nm (from Ag(+) : Pd(−) to Au(+) : Pd(−)), and their crystal sizes were comparable to those obtained by TEM. Furthermore, Pd(+) heterogeneous sparks (not shown in Fig. 7) show that the locations of their peaks were the same as the Pd(−) sparks but their intensities were changed due to the different metal fractions, as described in Table 4.

As discussed with the generation of monometallic particles, gaseous bimetal species from metal 1 and metal 2 electrodes are generated once a high temperature spark channel is formed. If the condensation temperature of metal 1 is higher than that of metal 2, the condensation of metal 1 vapor to liquid progresses more rapidly than that of metal 2 when these metal vapors are swept out from the spark channel by the nitrogen gas flow. During this process, liquid metal 1 can be pushed from the mixture vapor of metals 1 and 2 toward the interface, where the mixture is separated by the nitrogen gas, due to the temperature gradient between the mixture and nitrogen gas (Zheng, 2002). Simultaneously, metal 2 near the interface begins to condense into a liquid during the movement of metal 1. Further cooling by nitrogen gas flow can induce the solidification of the separately remaining liquid metals into two primary monometallic particles. These two monometallic particles then coagulate to form agglomerates (Borra, 2006).

4. Conclusions

The Ag, Pd, Pt, and Au monometallic particles were agglomerates with mean diameters of 14.9, 26.7, 37.7, and 48.8 nm, respectively, consisting of primary particles ranging in size from 2 to 4 nm (Ag < Pd < Pt < Au). The structure of these particles was fcc. The corresponding rates of particle generation were 0.12, 1.68, 16.00, and 40.30 μg/min. The higher ionization potential of an Au atom (9.22 eV) caused larger clusters and primary particles of Au. A hypothesis was suggested that there is a correlation between the generation rate and the ionization potential of a metal (Ag < Pd < Pt < Au). The bimetallic particles were found to be binary mixtures (not alloys) of two individual monometallic particles even though they had agglomerated. The composition of the bimetallic particles was measured at various combinations of materials and polarity of the spark electrode. The polarity of the electrodes in each bimetal combination strongly affected the size distribution. The rates of particle generation (or mass fractions of Pd) of Pd(+) : Pt(−), Pd(+) : Au(−), Pd(+) : Ag(−) were 2.64 (0.52), 3.78 (0.59), 0.66 (0.85) μg/min, respectively. However, the rates of particle generation (or mass fractions of Pd) were 6.28 (0.32), 6.88 (0.30), 0.28 (0.75) μg/min, respectively, when the polarity was switched. When the ionization potential of an anode material was higher than that of a cathode material, the hypothesis that there is a correlation between the ionization potential and the generation rate was valid. Even if the ionization potential of the anode material was lower than that of the cathode material, the generation rate of the anode metal particles was higher than that of the cathode metal particles. This might be caused by higher temperature channel formed near the anode and thus higher evaporation and subsequent nucleation/condensation near the anode. For Pd–Pt and Pd–Au sparks, the mass fractions of the anode materials were higher than those of the cathode materials. On the other hand, for the Pd–Ag sparks (Pd(+) : Ag(−) and Ag(+) : Pd(−)), Pd always had higher mass fraction than Ag regardless of the electrode polarity.

Acknowledgment

This study was supported by a Korea Institute of Environmental Science and Technology (KIEST) grant (013-071-052).

References

Artamonov, M. F., Krasov, V. I., & Paperny, V. L. (2001). Generation of multiply charged ions from a cathode jet of a low-energy vacuum spark. *Journal of Physics D*, *34*, 3364–3367.

Berkowitz, A. E., & Walter, J. L. (1987). Spark erosion: A method for producing rapidly quenched fine powders. *Journal of Materials Research*, *2*, 277–288.

Borra, J.-P. (2006). Nucleation and aerosol processing in atmospheric pressure electrical discharges: Powders production, coatings and filtration. *Journal of Physics D*, *39*, R19–R54.

Borra, J.-P., Goldman, A., Goldman, M., & Boulaud, D. (1998). Electrical discharge regimes and aerosol production in point-to-plane DC high-pressure cold plasmas: Aerosol production by electrical discharges. *Journal of Aerosol Science*, *29*, 661–674.

Byeon, J. H., Park, J. H., Yoon, K. Y., Ko, B. J., Ji, J. H., & Hwang, J. (2006). Removal of volatile organic compounds by spark generated carbon aerosol particles. *Carbon*, *44*, 2106–2108.

Devarajan, S., Bera, P., & Sampath, S. (2005). Bimetallic nanoparticles: A single step synthesis, stabilization, and characterization of Au–Ag, Au–Pd, and Au–Pt in sol–gel derived silicates. *Journal of Colloid and Interface Science*, *290*, 117–129.

Evans, D. E., Harrison, R. M., & Ayres, J. G. (2003). The generation and characterisation of elemental carbon aerosols for human challenge studies. *Journal of Aerosol Science*, *34*, 1023–1041.

Harada, M., Toshima, N., Yoshida, K., & Isoda, S. (2005). Aggregated structure analysis of polymer-protected platinum/ruthenium colloidal dispersions using EXAFS, HRTEM, and electron diffraction measurements. *Journal of Colloid and Interface Science*, *283*, 64–78.

Holland, L. (1956). Evaporation from an electric arc in vacuum. *Nature*, *178*, 328.

Horvath, H., & Gangl, M. (2003). A low-voltage spark generator for production of carbon particles. *Journal of Aerosol Science*, *34*, 1581–1588.

Kim, J.-T., & Chang, J.-S. (2005). Generation of metal oxide aerosol particles by a pulsed spark discharge technique. *Journal of Electrostatics*, *63*, 911–916.

Krasik, Y. E., Gleizer, S., Chirko, K., Gleizer, J. Z., Felsteiner, J., Bernshtam, V. et al. (2006). Characterization of a channel spark discharge and the generated electron beam. *Journal Applied Physics*, *99*, 063303-1–063303-14.

Lu, S.-Y., & Lin, Y.-Z. (2000). Pd–Ag alloy films prepared by metallorganic chemical vapor deposition process. *Thin Solid Films*, *376*, 67–72.

Marusina, V. I., & Filimonenko, V. N. (1984). Relationship between the thermal conditions of spark discharge and the particle shape and size distribution of a tungsten carbide micropowder. *Powder Metallurgy and Metal Ceramics*, *23*, 432–436.

Mizsei, J., Sipilä, S., & Lantto, V. (1998). Structural studies of sputtered noble metal catalysts on oxide surfaces. *Sensors and Actuators B*, *47*, 139–144.

Neogrády, P., Kellö, V., Urban, M., & Sadlej, A. J. (1997). Ionization potentials and electron affinities of Cu, Ag, and Au: Electron correlation and relativistic effects. *International Journal of Quantum Chemistry*, *63*, 557–565.

Oleshko, V. P. (2006). Aperiodic core structures of Pd and Pt giant clusters chemically stabilized with diphenyl phosphide ligands. *Journal of Molecular Catalysis A*, *249*, 4–12.

Quorum Technologies. (2007). *Sputtering Coating Technical Brief* ⟨http://www.quorumtech.com⟩.

Schwyn, S., Garwin, E., & Schmidt-Ott, A. (1988). Aerosol generation by spark discharge. *Journal of Aerosol Science*, *19*, 639–642.

Simonin, L., Lafont, U., Tabrizi, U., Schmidt-Ott, A., & Kelder, E. M. (2007). Sb/O nano-composites produced via spark discharge generation for Li-ion battery anodes. *Journal of Power Sources*, *174*, 805–809.

Wang, K.-W., Chung, S.-R., & Perng, T. P. (2006). Selective oxidation of Pd and compositional reconstruction in $Pd_{70}Ag_{30}$ alloy nanoparticles. *Journal of Alloys and Compounds*, *417*, 60–62.

Watters, Jr., R. L., DeVoe, J. R., Shen, F. H., Small, J. A., & Marinenko, R. B. (1989). Characteristics of aerosols produced by the spark discharge. *Analytical Chemistry*, *61*, 1826–1833.

Yang, C.-C., Wan, C.-C., & Wang, Y.-Y. (2004). Synthesis of Ag/Pd nanoparticles via reactive micelles as templates and its application to electroless copper deposition. *Journal of Colloid and Interface Science*, 433–439.

Zheng, F. (2002). Thermophoresis of spherical and non-spherical particles: A review of theories and experiments. *Advances of Colloid Interface Science*, *97*, 255–278.